Nationaal Lucht- en Ruimtevaartlaboratorium
National Aerospace Laboratory NLR

NLR-TP-2002-332

High cycle fatigue behaviour of intermetallic γ-TiAl based alloys

M.F.J. Koolloos, D.J. Arrell, M.B. Henderson and S. Gallet

Nationaal Lucht- en Ruimtevaartlaboratorium
National Aerospace Laboratory NLR

NLR-TP-2002-332

High cycle fatigue behaviour of intermetallic γ-TiAl based alloys

M.F.J. Koolloos, D.J. Arrell*, M.B. Henderson** and S. Gallet**

* ALSTOM Power Sweden AB, SE-612 82 Finspång, Sweden

** ALSTOM Power Technology Centre, Cambridge Road, Whetstone, Leicester LE8 6LH, UK

This report is based on a presentation held at the 7th Liège Conference: Materials for Advanced Power Engineering, at Liège, Belgium on 29 September - 2 October 2002.

Customer:	National Aerospace Laboratory NLR
Working Plan number:	1.1.B.1f
Owner:	National Aerospace Laboratory NLR
Division:	Structures and Materials
Distribution:	Unlimited
Classification title:	Unclassified
	June 2002

Contents

3 Tables
12 Figures

(15 pages in total)

Nomenclature

Roman symbols

K_t	stress concentration factor
R	stress ratio
$R_{0.2}$	yield strength
R_m	ultimate tensile strength
Z	area reduction after fraction

Greek symbols

σ_a	stress amplitude
σ_m	mean stress
σ_w	fatigue limit when $\sigma_m=0$
σ_d	fatigue limit when $\sigma_m\neq0$

Abbreviations

cgd	crack growth direction
FTR	fir tree root
HCF	high cycle fatigue
HIP	hot isostatic pressing
LCF	low cycle fatigue
LPT	low pressure turbine
OM	optical microscopy
SEM	scanning electron microscopy

HIGH CYCLE FATIGUE BEHAVIOUR OF INTERMETALLIC γ-TiAl BASED ALLOYS

M.F.J. Koolloos[a], D.J. Arrell [b], M.B. Henderson[c] and S. Gallet[c]

[a] National Aerospace Laboratory NLR, P.O.Box 153, 8300 AD Emmeloord, The Netherlands
[b] ALSTOM Power Sweden AB, SE-612 82 Finspång, Sweden
[c] ALSTOM Power Technology Centre, Cambridge Road, Whetstone, Leicester LE8 6LH, UK

Abstract

The high cycle fatigue behaviour of two versions of a high strength TiAl-based alloy (ABB-2 and ABB-23) have been investigated. The plain and notched (K_t = 3) axial high cycle fatigue behaviour of ABB-2 has been studied at 20 and 700°C under two different R ratios, and that of ABB-23 has been studied at 20°C (R=0.1 and 0.5) and 550°C (R=0.1). The fatigue tests showed flat S-N plots with high fatigue strength to UTS ratios (å1). The notched fatigue strength depended on the colony size relative to the specimen size and was often higher than the unnotched fatigue strength. The fatigue strength of both ABB alloys compare well with trendline data presented for Ti-4722XD however the degree of scatter in the endurance data is often excessive. The increased fatigue strength for ABB-2 and ABB-23 is commensurate with the increased tensile properties of the ABB alloys. After the fatigue tests metallographic investigation of fracture surface cross-sections was carried out to determine the fracture modes and fractography was done to reveal the initiation sites and crack growth directions. It is concluded that although both the ABB alloys show very high fatigue strength relative to their tensile strength, their behaviour strongly depends on the microstructure.

Keywords: Intermetallic, gamma TiAl, High Cycle Fatigue, Fractography, Microstructure

1. Introduction

Gamma based intermetallic TiAl alloys show great promise as candidate materials for gas turbine rotating parts exposed to intermediate temperatures, owing to their relatively low density compared with nickel-based alloys. In the temperature range from 20 to 750°C, titanium aluminides exhibit attractive density-corrected mechanical properties and a high oxidation resistance. However, the low ductility (<2% at room temperature) and fracture toughness of γ-TiAl are commonly recognised as its main drawbacks [1-4]. Much research has been done over the last decades to increase the ductility and improve the mechanical properties. This research has led to the development of titanium aluminides from simple Ti-48Al to several more complex alloys of Ti-(47-49)Al-(1-3)X_1-(1-10)X_2-(0-1)X_3 (in at.%) where X_1 = V, Cr, Mn; X_2 = Nb, Mo, Ta, Hf, W; and X_3 = Si, B, Fe, C, N [2,5-7]. Several investigations have shown that the microstructure greatly affects the mechanical properties [8]. Small changes in composition, casting and heat treatment procedures may cause changes in the microstructure and hence changes of material properties. It is therefore of utmost importance to perform detailed studies when a new alloy is being developed.

The γ-TiAl alloy ABB-2 with nominal composition Ti-46Al-2W-0.5Si (at.%) was developed in the framework of the European COST501 project (1994 to 1998) and several batches of material were characterised [9]. The present study has been conducted within COST522 (1999-2003), where specimens extracted from low pressure turbine (LPT) blades manufactured from the ABB-2 alloy have been characterised and compared with the properties for the new, fine grained ABB-23 alloy.

This article presents the results of an investigation on the high cycle fatigue (HCF) behaviour of ABB-2 and ABB-23. Axial HCF testing of ABB-2 has been conducted in air at 20 and 700°C at R=0.1 and 0.5, and ABB-23 has been tested at 20 and 550°C at R = 0.1 and 0.5. Both smooth and notched (K_t=3) specimens have been used. Post-test fractographic and metallographic examination of longitudinal cross-sections was conducted for a number of specimens to determine the fracture modes and reveal the initiation sites and crack growth directions.

2. Materials and experimental procedures

2.1 Materials

The materials used for the present study were ABB-2 and ABB-23, provided by ALSTOM Power (Switzerland). The materials were cast, HIPped (1260°C, 4h, 172 MPa) and heat-treated (1350°C for 1h followed by gas fan cool, then held at 1000°C for 6h and furnace cooled) resulting in a nearly lamellar structure. The ABB-2 alloy with nominal composition Ti-46Al-2W-0.5Si (at.%) was supplied in the form of a cast plate and sections removed from a LPT blade for an industrial gas turbine engine. It showed a generally inhomogeneous microstructure with large areas having a nearly lamellar microstructure, and a colony size of 0.5-2 mm. The ABB-23 alloy is an improved version of ABB-2, containing boron to homogenise and refine the microstructure. Its nominal composition is Ti-45Al-2W-0.55Si-0.6B (at.%) and it was supplied as round cast bars in two diameters.

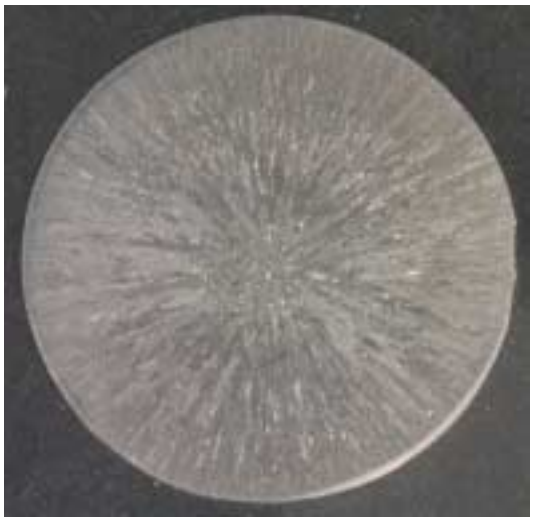

Figure 1. *Optical macrograph of ABB-23 Ø16 mm cast bar structure.*

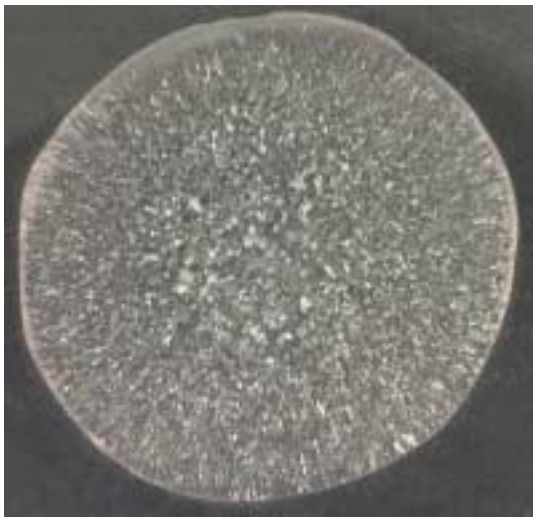

Figure 2. *Optical macrograph of ABB-23 Ø25 mm cast bar structure.*

The microstructure of ABB-23 was duplex with a small amount of equiaxed γ-TiAl grains. The colony size in the Ø16 mm bars (see Figure 1) varied from 20-50 μm at the centre of the bars to 200 μm near the edge of the bar. The colony size in the Ø25 mm bars (see Figure 2) was 200-300 μm over the entire cross-section. However, due to the casting process the shape of the colonies changed from equiaxed in the centre to columnar near the edge of the bar. Table 1 shows the actual compositions of the investigated materials.

Table 1. *Designation and composition (wt.%) of materials studied.*

Material	Batch	Ti	Al	W	Si	B	Fe	O	N
ABB-2	Plate	Bal.	30.5	9.1	0.33	-	0.023	0.066	0.032
ABB-2	FTR	Bal.	30.6	9.0	0.33	-	0.020	0.034	0.013
ABB-2	Blade	Bal.	30.6	9.0	0.33	-	0.020	0.034	0.013
ABB-23	1, Ø16mm	Bal.	29.6	9.3	0.38	0.163	0.022	0.053	0.013
ABB-23	1, Ø 25 mm	Bal.	29.6	9.3	0.38	0.163	0.022	0.053	0.013
ABB-23	2, Ø 16 mm	Bal.	29.9	9.1	0.41	0.193	0.044	0.071	0.011

FTR = Fir Tree Root

2.2 Testing Procedure

The plain specimen HCF behaviour of ABB-2 has been studied in air at 20 and 700°C at R = 0.1 and 0.5, and plain ABB-23 specimens (from two batches and two test bar diameters) have been tested at 20 and 550°C at R = 0.1 and 0.5. The notched (K_t = 3) behaviour for both alloys has been studied at 20°C and R = 0.1 only. Each sample was cycled until either failure or run-out, which was defined as 10^6 or 10^7 cycles depending on the test frequency used. For tests achieving run-out, the load was raised stepwise at each successive run-out until specimen failure occurred.

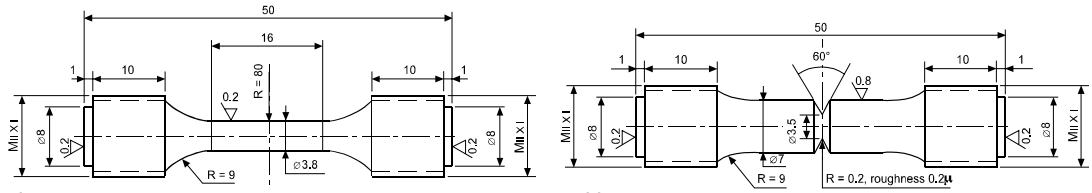

Figure 3. *Test specimens used for the NLR HCF tests. a) smooth, K_t=1; b) notched, K_t=3.*

Tests were carried out using 100 kN Amsler HFP machines, running at frequencies ranging from 90 to 160 Hz, depending on the loading conditions and specimen geometry (K_t =1 or 3) or using a 100kN Instron/Losenhausen servo-hydraulic test machine at 30 Hz (runout of 10^6 cycles). Figure 3 shows typical examples of the HCF specimens used in the study, which were machined from either the cast LPT blade (ABB-2), cast and HIPped slabs (ABB-2) or cast rods (ABB-23, Batches 1 and 2 as described above) as necessary.

To enable a baseline estimate of the HCF life to be made, room temperature tensile tests were also carried out using 250 kN and 100 kN Schenk Trebel test machines at a displacement rate of 1mm/min and 6%/min, respectively. Simple tensile specimens were used having a diameter of 7 mm (ABB-2 specimens) and 3.8 mm (ABB-23 specimens).

3. Results and Discussion

3.1 Tensile tests

The tensile test results showed large scatter within each batch and there was also batch-to-batch variation. Table 2 gives the average yield strength and ultimate tensile strength for some of the batches of ABB-2 and ABB-23.

Table 2. *Average room temperature tensile properties for batches of ABB-2 and ABB-23.*

Material	**Batch**	$R_{0.2}$ (MPa)	R_m (MPa)
ABB-2	FTR	491	507
ABB-2	Blade	523	619
ABB-23	1, Ø16mm	530	606

FTR = Fir Tree Root

3.2 HCF life

Figures 4 and 5 show the HCF results for ABB-2 (FTR + blade) and ABB-23 (all batches) respectively, both for R=0.1. The main body of data presented in Figure 4 are derived from the fir tree root (FTR) specimens. The tests with the ABB-2 blade specimens (K_t=1 only) are pointed out.

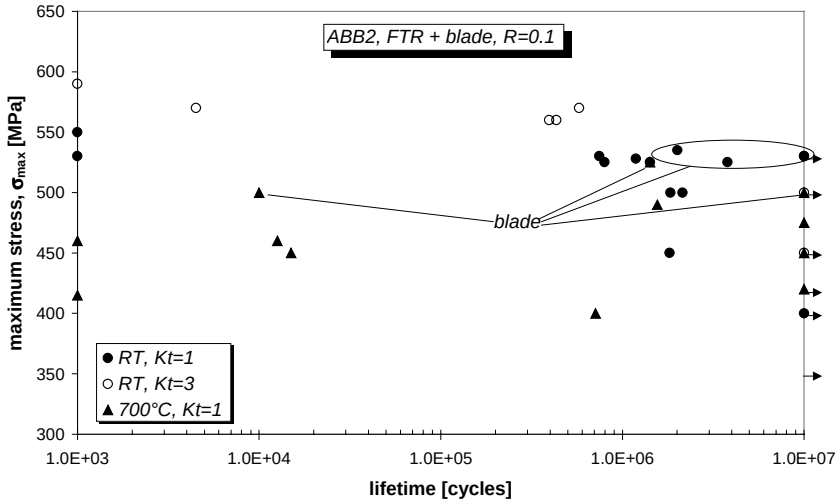

Figure 4. *Fatigue life for ABB-2 with R=0.1, K_t=1 or 3, at 20 and 700°C. Run-out at 10^7 cycles*

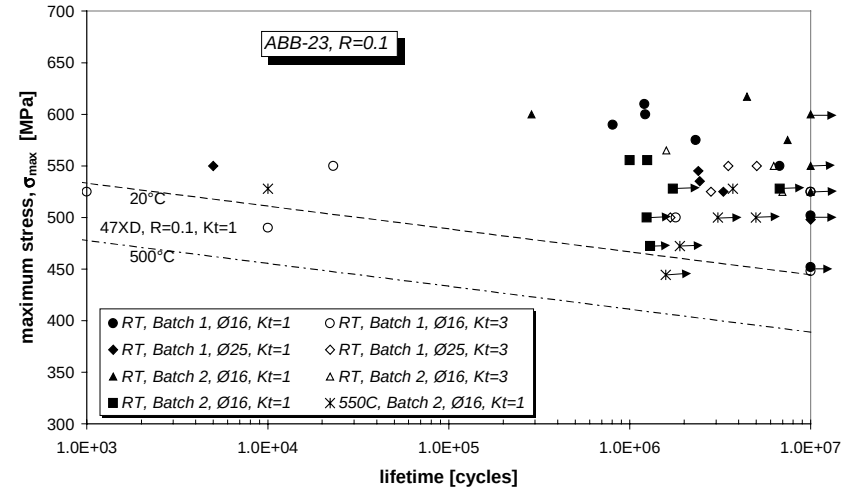

Figure 5. *Fatigue life of ABB-23 for R=0.1, K_t=1 at 20 and 550°C and K_t = 3 at 20°C. Run-out at 10^7 cycles. Trend lines for Ti-47-2-2XD at 20 and 500°C are added for comparison.*

The unnotched ABB-2 specimens show very flat fatigue curves with a high fatigue strength to R_m ratio (~1). The 700°C fatigue strength is lower than that at 20°C, although the tensile strength is fairly temperature independent at temperatures up to 700°C [8]. Apparently the fatigue strength decrease with temperature is not due to a decrease in R_m, but to a change in fatigue cracking mechanism (see Section 3.3). The fatigue strength of the notched ABB-2 specimens is higher than that of the unnotched specimens. This remarkable result can be explained by consideration of the coarse colony size in these castings (see Section 3.3). Furthermore, it is seen that the fatigue strength of the ABB-2 blade specimens is slightly higher than that of the ABB-2 FTR specimens, both at 20°C and at 700°C. This is probably caused by the difference in microstructure, which is known to have a large effect on the mechanical properties [8].

The ABB-23 alloy also shows very flat fatigue endurance curves (Figure 5) with a high fatigue strength to R_m ratio (~1). The fatigue strength for the unnotched ABB-23 specimens is higher than that of ABB-2, which corresponds with the higher tensile strength. Generally, the specimens from the Ø16 mm bars, batches 1 and 2, show similar fatigue behaviour, both for unnotched and for notched specimens. Unlike that found for ABB-2, the ABB-23 notched fatigue strength is lower than that for the unnotched specimens. The Ø25 mm bar specimens, Batch 1, show somewhat lower unnotched fatigue strengths compared with the Ø16 mm bar specimens and a notched fatigue strength similar to that of the unnotched specimens. This can be attributed to the larger colony size in the ABB-23 Ø25 mm bars. Increasing the test temperature to 550°C causes a reduction in fatigue strength in ABB-23 of similar magnitude as in Ti-47-2-2XD for which the trend lines are presented.

Figure 6 shows the plain specimen fatigue results for ABB-2 (blade) and ABB-23 (batch 1) at 20°C and R = 0.5. For both alloys the HCF curves are very flat, giving a transition from HCF to short life LCF behaviour over a cyclic stress range of around 10 MPa. The high R-ratio fatigue strength of ABB-2 is greater than that for ABB-23.

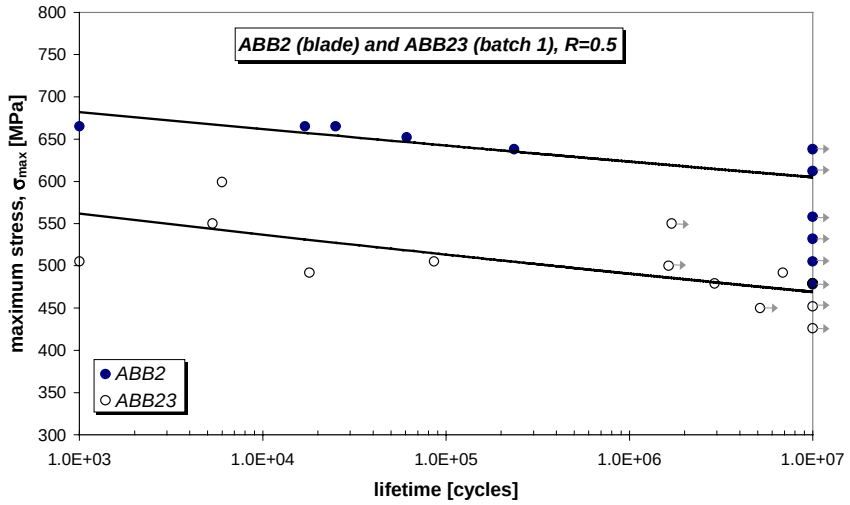

Figure 6. *Fatigue life of ABB2 and ABB23 at 20°C and R = 0.5. Run-out at 10^7 cycles.*

The S-N curves for all tested batches are much flatter than the curves for most metallic materials. This can be attributed to the small interval between $\Delta K_{threshold}$ and the fracture toughness, *i.e.* limited stable crack growth [9, 10]. Although the material exhibits little damage tolerance, the fatigue strengths are high compared to most other metallic alloys.

In highly loaded applications, *e.g.* rotating components in the low pressure stage of gas turbine engines, the inherent brittleness of γ-TiAl alloys requires the use of the so-called initiation based design. However, the S-N curve approach is of limited relevance to predict the fatigue limit since defects and small cracks (*e.g.* due to foreign object damage, FOD) can have a substantial effect on the fatigue strength [11].

Haigh diagrams

In order to compare the different fatigue tests, all results are plotted on a Haigh diagram (Figures 7 and 8) along with the Goodman lines for the ultimate tensile strength ($\sigma_m+\sigma_a=R_m$) and the 'first guess' life estimate using Hempels equation, as follows:

$$\sigma_D = \sigma_W \left\{ 1 - \sigma_m \cdot \frac{1-Z}{R_m} \right\} \tag{1}$$

where σ_m is the mean stress under HCF, R_m is the ultimate tensile strength, σ_w is the fatigue limit when σ_m =0, often taken to be 0.45R_m, σ_d is the fatigue limit when σ_m Í 0 and Z is the area reduction after fracture in a tensile test. For ABB2 two Goodman lines and two Hempel lines are drawn. This is because the R=0.1 data are based on specimens from the FTR and the R=0.5 data are based on specimens from the blade. Since the tensile properties differed for these two parts of the blade, the Goodman and Hempel lines differ also.

Haigh diagrams are usually considered to be a convenient method for extrapolating the fatigue behaviour from one R ratio to another, thereby limiting the amount of mechanical testing needed to construct a fatigue limit surface. However, the data in figures 7 and 8 show that there can be some discrepancies and inconsistencies. Figure 7 shows that the ABB-2 R=0.1 data fall below the FTR Goodman line, but the R=0.5 data agree well with the blade Goodman line. Figure 8 shows that the ABB-23 R=0.1 and R=0.5 data fall below the Goodman line, especially the R=0.5 data. This latter result is rather unexpected, as a finer grain structure is generally considered to improve the mechanical properties, whereas the effect of grain refinement shown here is the opposite (compare to R=0.5 data of ABB-2, figure 7). Thus, not only are there discrepancies of fits to the Goodman lines, but comparison of the two materials shows that for ABB-2 the R=0.5 fatigue strength is relatively higher than the R=0.1 fatigue strength, while for ABB-23 the opposite is true.

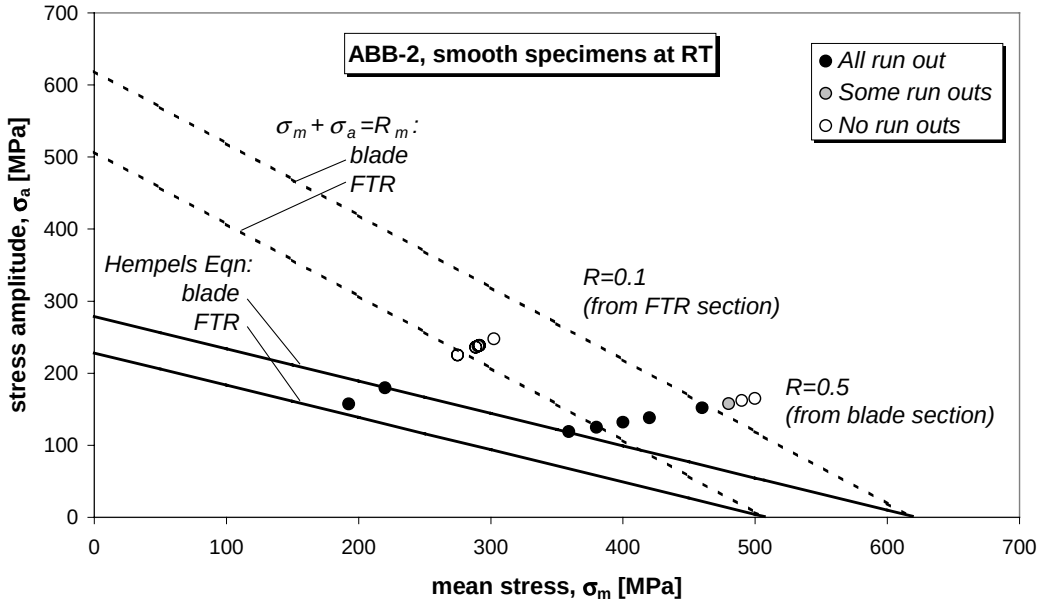

Figure 7. *Haigh diagram for ABB-2 with Goodman lines and Hempels equation lines.*

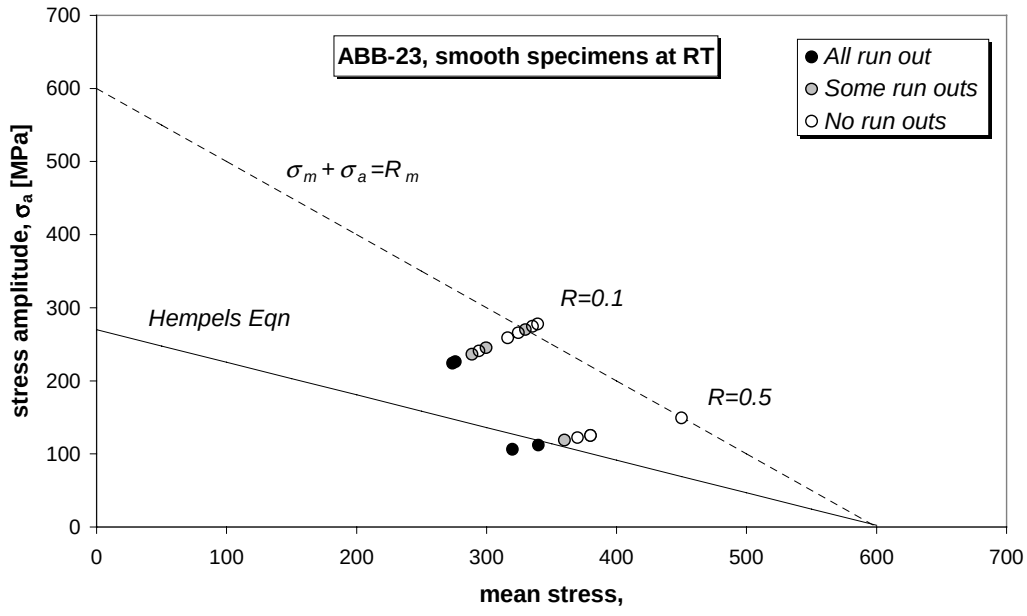

Figure 8. *Haigh diagram for ABB-23 (batch 1) with Goodman line and Hempels equation line.*

1.3 Fracture surfaces

Longitudinal sections

To reveal the fracture path, post-test, cross-sectional samples were prepared from a number of specimens and investigated using Optical Microscopy (OM) and Scanning Electron Microscopy (SEM). Figure 9 shows a cross-section through the fracture surface of an ABB-2 FTR specimen, tested at 20°C and R = 0.1. It can be seen that fracture occurred by transgranular failure of the lamellar colonies: interlamellar failure when the lamellae were oriented favourably, *i.e.* within an envelope of ±45° with the ideal plane of fracture (perpendicular to loading direction), and translamellar when the lamellae were oriented outside this envelope. At 700°C, not shown here, fracture occurred in a mixed intergranular / transgranular mode.

A large lamellar colony with favourably oriented lamellae and situated at or near the free surface was found to be detrimental to the fatigue strength. This is because the colony size is larger than the expected critical crack size resulting in instant failure after initiation [10]. The large colonies have also a size effect in the notched specimens: the notched area of the K_t=3 specimens is small, and so is the probability of the presence of a large colony with favourably oriented lamellae. Hence cracks are forced to initiate translamellarly, and the fatigue strength will be higher than in the unnotched specimens.

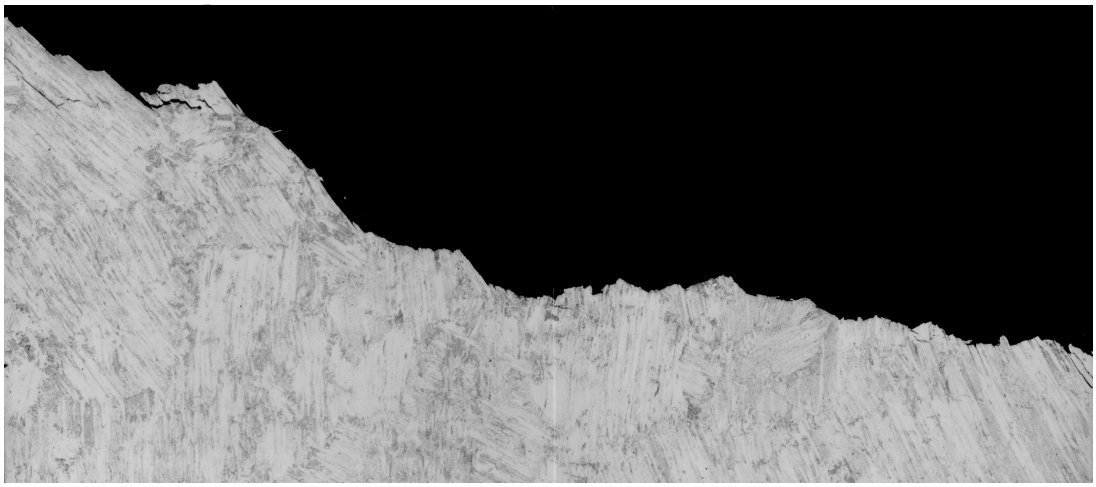

Figure 9. *Cross-section (OM) of fracture surface of unnotched ABB-2 specimen, tested at 20°C and R= 0.1.*

The ABB-23 colony size was too small to reveal the crack path by optical microscopy and hence SEM was used to analyse the cross-section. Figure 10 shows a cross-section through the fracture surface of an ABB-23 batch 1 Ø16 mm specimen, tested at 20°C and R = 0.1. Again, there is a strong tendency for transgranular fracture of lamellar colonies and γ-grains. This is notably observed by inspection of secondary cracks. Also, there is a tendency for interlamellar fracture when the lamellae are oriented favourably. However, this is less so than for ABB-2.

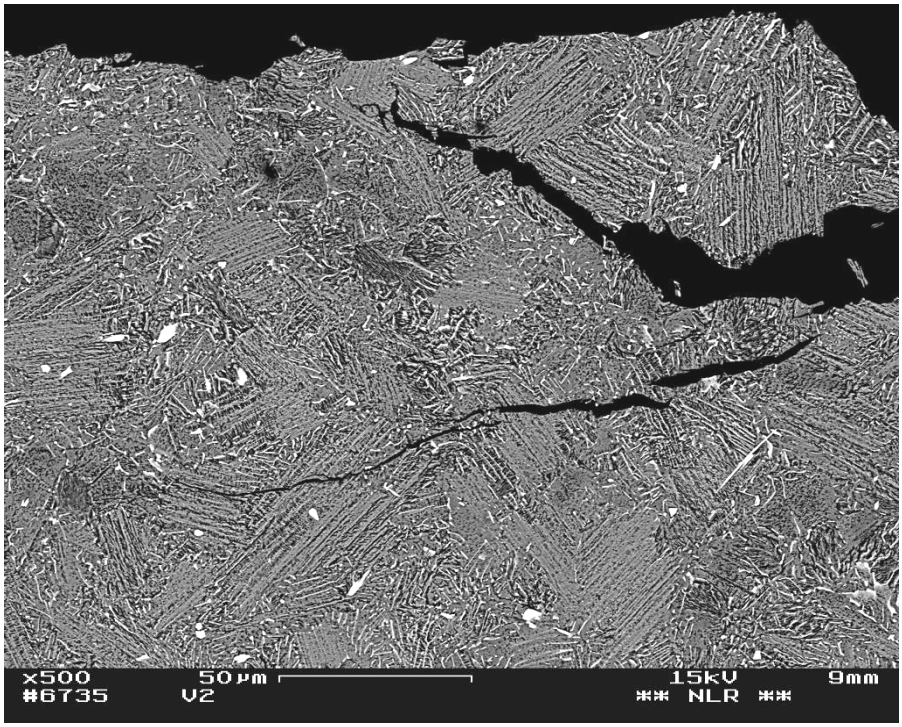

Figure 10. *Cross-section (SEM, Back Scattered Electron) of fracture surface of unnotched ABB-23 specimen, tested at 20°C and R = 0.1.*

Fractography

The ABB-2 (FTR) and ABB-23 (batch 1, Ø16 mm) fracture surfaces were investigated by stereo microscopy, for first impression and global fatigue crack features, and by SEM for more detailed investigation. Table 3 summarises the results.

Table 3. *Summary of fractographic examinations.*

	Stereo Microscopy	**SEM**
ABB-2	• very rough fracture surface • large faceted grains visible (interlamellar fracture) • no observable indications for crack initiation and cgd*	• practically no indication for crack initiation and cgd* • interlamellar fractured grains observed, but no river patterns indicating cgd*
ABB-23	• crack initiation region traceable • indications for global cgd* (see figure 11)	• global cgd* still visible • crack initiation site retraceable • local average cgd*, deduced from river patterns on transgranular fractured γ-grains (see Figure 12), agrees with global cgd*

** cgd = crack growth direction*

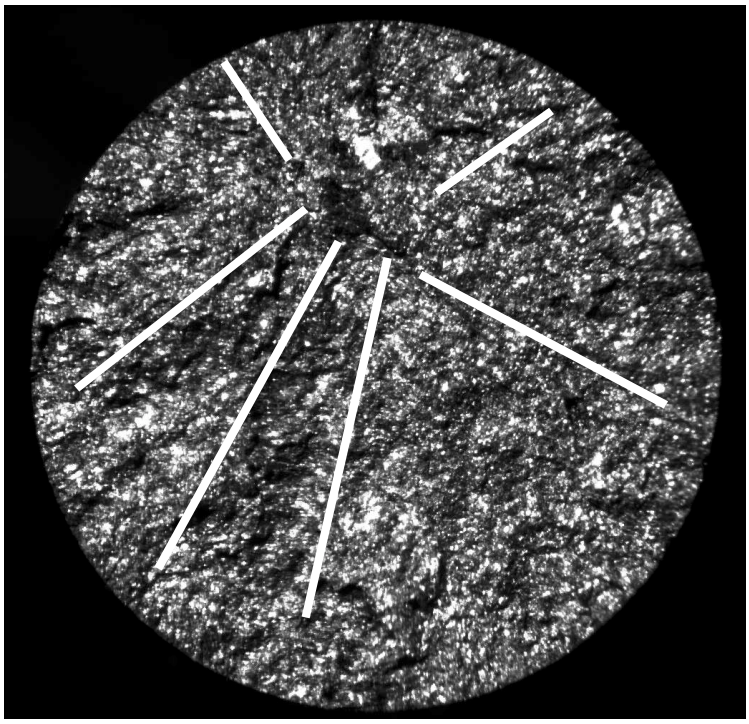

Figure 11. *Fracture surface (Optical Microscopy) of unnotched ABB-23 specimen tested at 20°C. Crack initiation region is clearly visible and global crack growth direction is indicated.*

4. Conclusions

- ABB-2 and ABB-23 show both at 20°C and at 700°C flat fatigue curves with a high fatigue strength to UTS ratio, due to the limited stable crack growth regime.
- For R=0.1 the unnotched fatigue strength of ABB23 is higher than that of ABB-2. For R=0.5 the unnotched fatigue strength of ABB23 is lower than that of ABB-2.
- For R=0.1 the notched fatigue strength of ABB-23 is lower than that of ABB-2. The reason for this is a size effect (notch area vs. lamellar colony size).
- Fracture was predominantly transgranular in both alloys, with interlamellar fracture for colonies with favourably oriented lamellae.
- Fatigue crack features on transgranular fractured grains were visible for ABB23 (γ-grains) but not for ABB2.
- For highly loaded applications in gas turbines knowledge of the effect of defects and cracks on the fatigue strength is essential.

Acknowledgements
The authors thank Alstom Power Switzerland for providing the test material and performing some of the tensile tests.

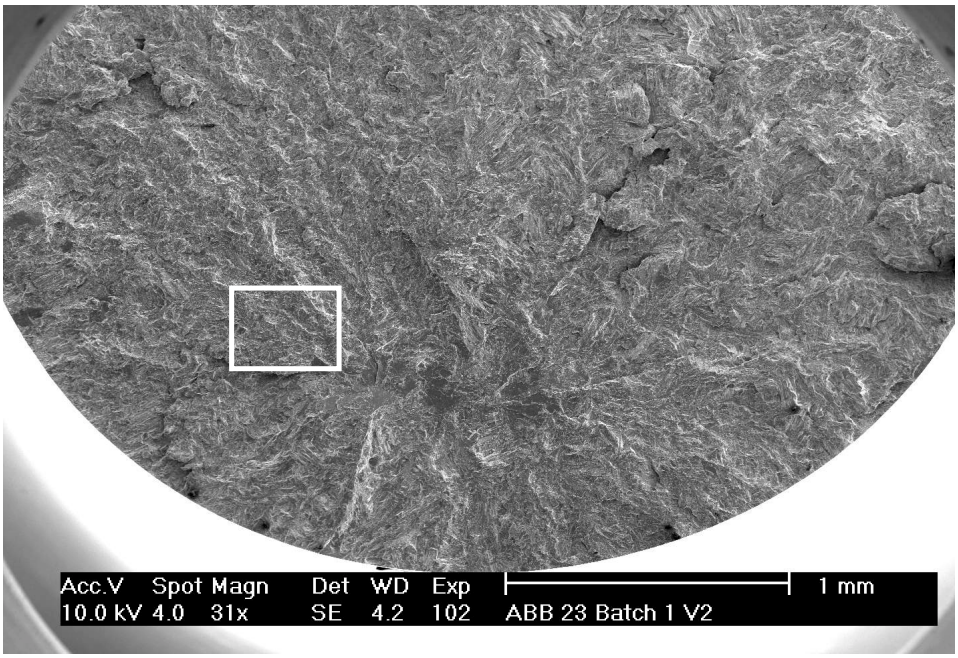

a)

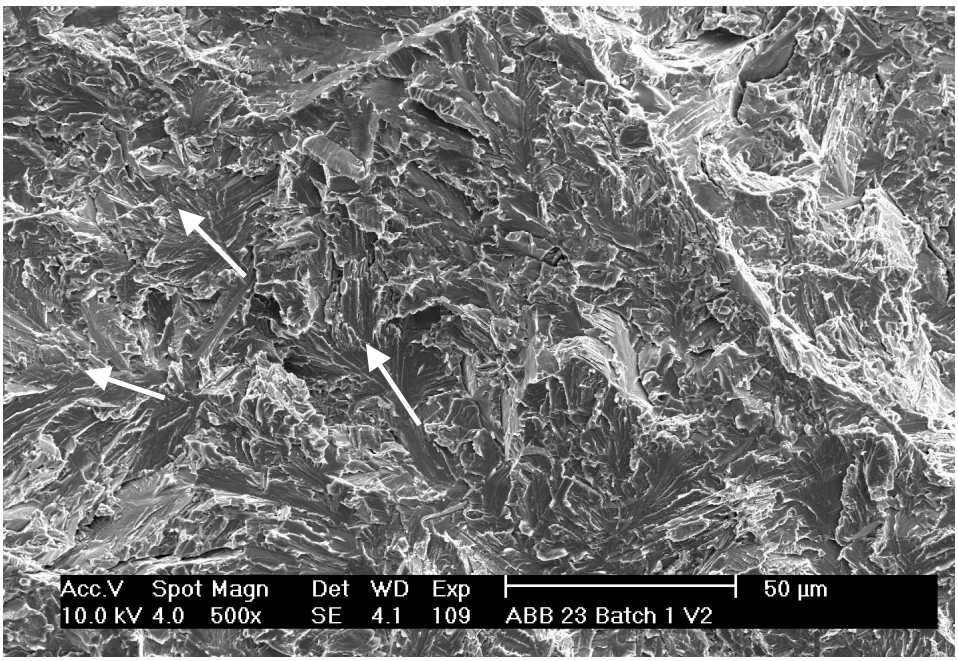

b)

Figure 12. *Fracture surface (SEM) of unnotched ABB-23 specimen, tested at 20°C. a) overview of crack initiation area; b) detail of area above and left of the initiation site. Crack growth directions are indicated on river patterns on transgranular fractured γ-grains.*

References

[1] Y.W. Kim and D.M. Dimiduk, "Progress in the Understanding of Gamma Titanium Aluminides," *JOM*, Vol. 43, 1991, pp. 40-47.

[2] Y.W. Kim, "Ordered Intermetallic Alloys, Part III: Gamma Titanium Aluminides," *JOM*, Vol. 46, 1994, pp. 30-39.

[3] I.J. Perrin, "Designing with Low Ductility Intermetallic Alloys," *Gas Turbines – Materials Make the Difference*, Workshop at DERA Farnborough, Hampshire, UK, 21/22 January 1999.

[4] D.M. Dimiduk, "Gamma Titanium Aluminide Alloys – an Assessment within the Competition of Aerospace Structural Materials," *Mater. Sci. Eng.*, Vol. A263, 1999, pp. 281-288.

[5] T.T. Cheng, M.R. Willis and I.P. Jones, "Effect of Major Alloying Additions on the Microstructure and Mechanical Properties of γ-TiAl," *Intermetallics*, Vol. 7, 1999, pp.89-99.

[6] F.S. Sun, C.X. Cao, S.E. Kim, Y.T. Lee and M.G. Yan, "Alloying Mechanism of Beta Stabilisers in a TiAl Alloy," *Metall. Mater. Trans. A*, Vol. 32A, 2001, pp. 1573-1589.

[7] H. Clemens, A. Lorich, N. Eberhardt, W. Glatz, W. Knabl, and H. Kestler, "Technology, Properties and Applications of Intermetallic γ-TiAl Based Alloys," *Z. Metallkd.* Vol. 90, 1999, pp. 569-580.

[8] V. Recina and B. Karlsson, "Tensile Properties and Microstructure of Ti-48Al-2W-0.5Si γ-Titanium Aluminide at temperatures between room temperature and 800°C," *Mater. Sci. Technol.*, Vol. 15, 1999, pp. 57-66.

[9] M. Nazmy and V. Lupinc, "Gamma TiAl Intermetallic for Gas Turbine Applications," *Proc. 6th Liège Conference, Part II*, J. Lecomte-Beckers, F. Schubert and P.J. Ennis (Ed.), 1998, pp. 933-944.

[10] V. Recina and B. Karlsson, "High Temperature Low Cycle Fatigue Properties of Ti-48Al-2W-0.5Si gamma Titanium Aluminide," *Mater. Sci. Eng.*, Vol. A262, 1999, pp. 70-81.

[11] M. Nazmy, M. Staubli, G. Onofrio and V. Lupinc, "Surface Defect Tolerance of a Cast TiAl Alloy in Fatigue," *Scripta Materialia*, Vol. 45, 2001, pp. 787-792